Real-time digital signal processing for live electro-optic imaging

Kiyotaka Sasagawa[1,2], **Atsushi Kanno**[1], **and Masahiro Tsuchiya**[1]

[1]*National Institute of Information and Communications Technology, 4-2-1 Nukui-Kitamachi, Koganei, Tokyo, 184-8795 Japan*
[2]*Graduate School of Materials Science, Nara Institute of Science and Technology, 8916-5 Takayama, Ikoma, Nara, 630-0192 Japan*
mtsu@nict.go.jp,sasagawa@ms.naist.jp

Abstract: We present an imaging system that enables real-time magnitude and phase detection of modulated signals and its application to a *Live Electro-optic Imaging* (LEI) system, which realizes instantaneous visualization of RF electric fields. The real-time acquisition of magnitude and phase images of a modulated optical signal at 5 kHz is demonstrated by imaging with a Si-based high-speed CMOS image sensor and real-time signal processing with a digital signal processor. In the LEI system, RF electric fields are probed with light via an electro-optic crystal plate and downconverted to an intermediate frequency by parallel optical heterodyning, which can be detected with the image sensor. The artifacts caused by the optics and the image sensor characteristics are corrected by image processing. As examples, we demonstrate real-time visualization of electric fields from RF circuits.

OCIS codes: (280.4788) Optical sensing and sensors; (100.0118) Imaging ultrafast phenomena; (040.2840) Heterodyne; (230.2090) Electro-optical devices; (350.4010) Microwaves.

References and links

1. K. Sasagawa, A. Kanno, T. Kawanishi, and M. Tsuchiya, "Live electro-optic imaging of microwave near-fields via ultra-parallel photonic heterodyne," IEEE *2007 MTT-S International Microwave Symposium Digest*, 401-404 (2007).
2. K. Sasagawa, A. Kanno, T. Kawanishi, and M. Tsuchiya, "Live electro-optic imaging system based on ultra-parallel photonic heterodyne for microwave near-fields," IEEE Trans. Microwave Theory Tech. **55,** 2782-2791 (2007).
3. K. Sasagawa, A. Kanno, and M. Tsuchiya, "Instantaneous Visualization of K-Band Electric Near-Fields by Live Electrooptic Imaging System Based on Double Sideband Suppressed Carrier Modulation," J. Lightwave Technol. **26,** 2782-2788 (2008).
4. A. Kanno, K. Sasagawa, and M. Tsuchiya, "W-Band live electro-Optic imaging system," presented at European Microwave Conf. 2008, the Netherlands, 27-31 Oct. 2008.
5. K. Sasagawa, and M. Tsuchiya, "Real-time monitoring system of RF near-field distribution images on the basis of 64-channel parallel electro-optic data acquisition," IEICE Electron. Express **2,** 600-606 (2005).
6. A. Kanno, K. Sasagawa, and M. Tsuchiya, "Instantaneous microwave transmission imaging of aqueous samples," presented at 2007 IEEE Int. Topical Meeting Microwave Photon., Canada, 3-5 Oct. 2007.
7. F. Pockels, "Lehrbuch der Kristalloptik," Teubner, Leipzig (1906).
8. J. A. Valdmanis, G. Mourou, and C. W. Gabel, "Picosecond electro-optic sampling system," Appl. Phys. Lett. **41,** 211-212 (1982).
9. K. J. Weingarten, M. J. W. Rodwell, and D. M. Bloom, "Picosecond optical sampling of GaAs integrated circuits," IEEE J. Quantum Electron. **24**, 198-220 (1988).
10. T. Nagatsuma, "Measurement of high-speed devices and integrated circuits using electro-optic sampling technique," IEICE Trans. Electron. **76-C,** 55-63 (1993).

#113871 - $15.00 USD Received 7 Jul 2009; revised 2 Aug 2009; accepted 7 Aug 2009; published 19 Aug 2009

11. A. Sasaki, and, T. Nagatsuma, "Electric-field scanning system using electro-optic sensor," IEICE Trans. Electron. **E86-C,** 1345-1351 (2003).
12. M. Takahashi, E. Suzuki, S. Arakawa, H. Ota, K. Arai, and R. Sato, "High speed system for measureing electromagnetic field distribution," IEICE Trans. Commun. **E89-B,** 2905-2911 (2006).
13. S. Wakana, T. Ohara, M. Abe, E. Yamazaki, M. Kishi, and M. Tsuchiya, "Fiber-edge electrooptic/magnetooptic probe for spectral-domain analysis of electromagnetic field," IEEE Trans. Microwave Theory Tech. **48,** 2611-2616 (2000).
14. M. Iwanami, M. Nakada, H. Tsuda, K. Ohashi, and J. Akedo, "Ultra small electro-optic field probe fabricated by aerosol deposition," IEICE Electron. Express **4,** 26-32 (2007).
15. D.-J. Lee and J. F. Whitaker , "An optical-fiber-scale electro-optic probe for minimally invasive high-frequency field sensing," Opt. Express **16,** 21587-21597 (2008), http://www.opticsinfobase.org/oe/abstract.cfm?URI=oe-16-26-21587.
16. H. Togo, N. Shimizu, and T. Nagatsuma, "Near-field mapping system using fiber-based electro-opticprobe for specific absorption rate measurement," IEICE Trans. Electron., **E90-C**, 436-442 (2007).
17. K. Yang, G. David, J.-G. Yook, I. Papapolymerou, L. P. B. Katehi, and J. F. Whitaker, "Electrooptic mapping and finite-element modeling of the near-field pattern of a microstrip patch antenna," IEEE Trans. Microwave Theory Tech. **48,** 288-293 (2000).
18. K. Sasagawa, and M. Tsuchiya, "Low noise and high frequency resolution electrooptic sensing of RF near-fields using an external optical modulator," J. Lightwave Technol. **26,** 1242-1248 (2008).
19. D. J. Lee, and J. F. Whitaker, "Bandwidth enhancement of electro-optic field sensing using photonic down-mixing with harmonic sidebands," Opt. Express **16,** 14771-14779 (2008), http://www.opticsinfobase.org/oe/abstract.cfm?URI=oe-16-19-14771.
20. K. Sasagawa, and M. Tsuchiya, "Modulation depth enhancement for highly sensitive electrooptic RF near-field measurement," Electron. Lett. **42,** 1357-1358 (2006).

1. Introduction

By virtue of the recent progress in integrated circuits, performances of image sensors and digital signal processors (DSPs) have been improved. State-of-the-art complementary-metal-oxide-semiconductor (CMOS) image sensors capture 100 $\times$ 100 pixel images with a frame rate exceeding 10 000 frames / s. A commercially available DSP based on a field-programmable gate array enables real-time digital processing. By combining these systems, highly sensitive lock-in imaging can be realized.

One of the application of the lock-in imaging is the live electro-optic imaging (LEI) system, which enables real-time visualization of RF electric near-fields at microwave and millimeter wave frequencies [1–5]. Figure 1 sketches the concept. Intensity and phase images of the electric fields of a device-under-test are acquired continuously at video rate. One of the promising applications of LEI is diagnosis of microwave circuits where electromagnetic interference must be carefully considered. It is also expected that LEI could be applied to image analysis of materials [6].

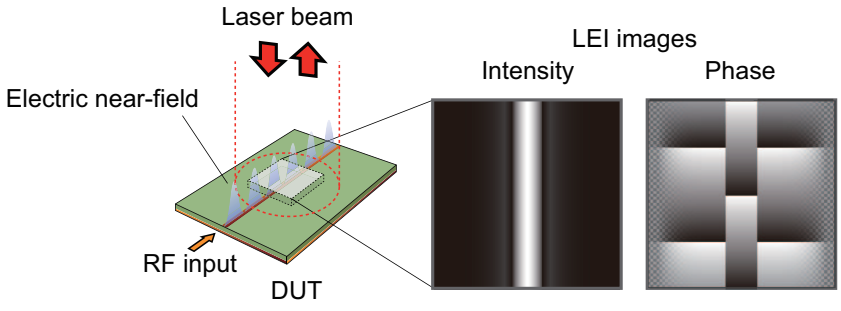

Fig. 1. Concept of LEI where DUT is the device under test.

In this paper, we report a real-time imaging system for lock-in detection composed of a high-

#113871 - $15.00 USD Received 7 Jul 2009; revised 2 Aug 2009; accepted 7 Aug 2009; published 19 Aug 2009

speed image sensor and a digital signal processor (DSP) for application to LEI. The system achieves sensitivity sufficient to observe electric field signals via the EO effect. Some movies of electric near-fields above microwave circuits captured by the LEI system are presented.

2. Live Electro-optic Imaging

In this section, we describe the LEI system, which uses a high-speed CMOS image sensor and a DSP. In the LEI system, electric field signals are converted to optical signals by the Pockels effect [7] and detected by an image sensor. The measurement principle is shown in Fig. 2. An EO crystal consisting of a ZnTe crystal plate is used as an electric-field sensor. Its birefringent characteristics are affected by an applied electric field. The optical polarization of light passing through the crystal is modulated by the electric field. That modulation is converted to an intensity modulation by an optical analyzer. Finally, the output signal is detected by a photodiode.

In conventional electro-optic systems, an optical beam is focused on the measurement point in an EO crystal and scanned to acquire an electric field image [8–17] On the other hand, in the LEI system, all sample points are measured in parallel by an optical image sensor. Therefore, the image acquisition time is reduced drastically and real-time imaging at video rates is achieved [1, 2].

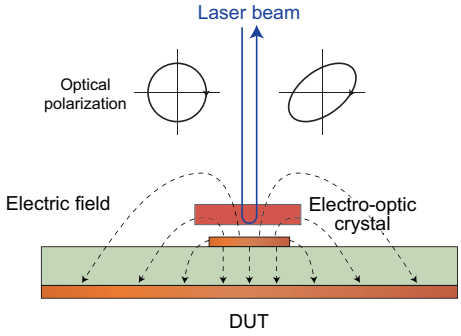

Fig. 2. Electric field sensing based on the Pockels effect.

Figure 3 shows the experimental setup. The image sensor is a high-speed CMOS image sensor based on silicon technology (micam GEN from BrainVision). The number of pixels of the image sensor is 10 000 and the frame rate is 20 kHz. The optical intensity on each pixel is output as a 14-bit digital signal. The light source is a single-mode laser diode at 780 nm where the Si-based image sensor has high sensitivity. The reference signal from the image sensor module is fed into the signal generators.

The frame rate of the image sensor is much lower than the RF frequency of the electric field, which is in the microwave range. Therefore, the RF signal is downconverted by an optical heterodyning method [18, 19]. Light launched from the laser source is modulated by a Mach-Zehnder modulator at a frequency of f_{LO}. Next, the polarization of the light is modulated again in the EO crystal at the frequency of the measured electric field f_{RF}. The typical power of the modulated light is approximately 4 mW. The polarization modulation is converted to an intensity modulation by a polarization beamsplitter. The waveplates are adjusted to obtain highest sensitivity [20]. The output light includes the intermediate frequency component $f_{\mathrm{IF}} = |f_{\mathrm{RF}} - f_{\mathrm{LO}}|$ whose intensity and phase reflect those of the electric field signal. Here, f_{LO} is chosen so that f_{IF} is lower than the Nyquist frequency of the image sensor. In the present system, f_{IF} is set to 5 kHz, The intermediate frequency is quarter of the image sensor frame

#113871 - $15.00 USD Received 7 Jul 2009; revised 2 Aug 2009; accepted 7 Aug 2009; published 19 Aug 2009

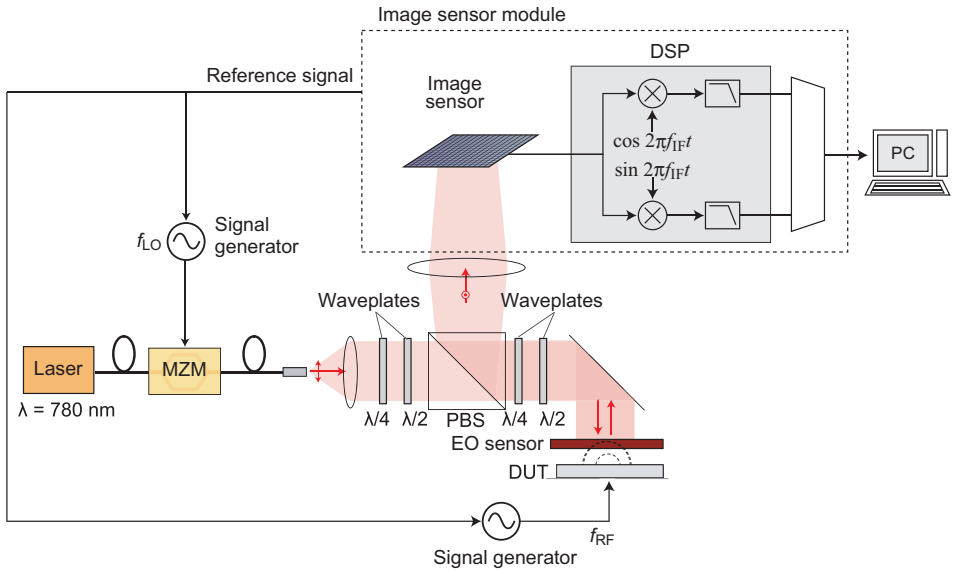

Fig. 3. Setup of LEI system where MZM: Mach-Zehnder modulator, PBS: polarization beamsplitter, EO sensor: electro-optic sensor, DSP: digital signal processor, PC: personal computer.

rate. The reference signal is generated in the image sensor module and input into the signal generators. The detected signal on each pixel of the image sensor is processed by a DSP and an electric field image is displayed on a PC. Further details of the LEI system are described in Ref. [2].

3. Signal processing by lock-in detection

The most important advantage of LEI is its high-speed image acquisition and real-time imaging. To achieve it, it is necessary to obtain the electric field signal from each pixel of the image sensor simultaneously. The image sensor used in the present LEI system outputs 10 000 pixels with 14-bit depth every 50 microseconds. The data are first processed by a digital signal processor and filtered to reduce the data size. Next, the electric field magnitude and phase images are extracted and artifacts of the sensitivity and phase are corrected on the PC. Finally, the images are displayed. In this section, we describe the operation of each process.

3.1. Field magnitude and phase detection

The field magnitude and phase at the intermediate frequency f_{IF} in each pixel are measured by the LEI system. In other words, two-phase lock-in detection imaging is performed by the combination of the high-speed CMOS image sensor and the DSP.

The intermediate frequency is 5 kHz. The frame rate of the image sensor is 20 kHz. Thus, 4 frames correspond to one period of the intermediate frequency. The received signals in one period $u_n(n = 1, \cdots, 4)$ are converted to digital signals and input into a digital signal processor (DSP). In the DSP, each of two reference rectangular-wave signals with a phase difference of $\pi/2$ are multiplied by the measured signal. The reference signals are given by (1, 1, -1, -1) and (-1, 1, 1, -1) for each period. The results $v_{\cos}$ and $v_{\sin}$ are the cosine and sine components of the

#113871 - $15.00 USD Received 7 Jul 2009; revised 2 Aug 2009; accepted 7 Aug 2009; published 19 Aug 2009

signal given by

$$v_{\cos}(m) = u_{4m+1} + u_{4m+2} - u_{4m+3} - u_{4m+4} \tag{1}$$

$$v_{\sin}(m) = -u_{4m+1} + u_{4m+2} + u_{4m+3} - u_{4m+4}, \tag{2}$$

where m is the period number and u_i is the measured signal of frame number i.

The intermediate frequency is converted to a DC component. By accumulating all frames, low-pass filtering is performed,

$$V_{\cos} = \sum_{m=1}^{N/4} v_{\cos}(m) \tag{3}$$

$$V_{\sin} = \sum_{m=1}^{N/4} v_{\sin}(m), \tag{4}$$

where N is the number of the accumulated frames. By this operation, the data sizes are reduced. Its reduction ratio is $R = f_{\mathrm{IS}}/f_{\mathrm{LEI}}$ where f_{IS} and f_{LEI} are the frame rates of the high-speed image sensor and of the LEI, respectively. The output data are transferred to the PC. The field magnitude M and phase ϕ are

$$M = V_{\cos}^2 + V_{\sin}^2 \tag{5}$$

$$\phi = \arctan \frac{V_{\sin}}{V_{\cos}}. \tag{6}$$

These operations are performed in each pixel and a pair of field magnitude and phase images are obtained.

3.2. Field magnitude correction

The light modulated by the optical intensity modulator is expanded and illuminated on the EO crystal as a Gaussian beam. There is thus an optical intensity difference between the center and periphery of the crystal. In addition, interference fringes between the image sensor chip and the cover glass are superimposed on the image. These result in a nonuniform sensitivity in the observation area, which is corrected by image processing as described below.

The optical power of the intermediate frequency component corresponding to the measured field magnitude signal is

$$I_{\mathrm{IF}}(t) = \frac{|r|^2 I_0 a^2}{2} \cos 2\pi (f_{\mathrm{LO}} - f_{\mathrm{RF}})t, \tag{7}$$

where I_0 is the input optical intensity r is the total amplitude transmittance of the optical system, a and f_{RF} are the amplitude and frequency of optical modulation by the RF electric field via the Pockels effect, and f_{LO} is the local oscillator frequency. The further details are described in Ref. [2]. Equation (7) indicates that the measured signal is proportional not only to the electric field magnitude but also to the optical power. Therefore, artifacts appear in a LEI image if the illuminated beam is nonuniform.

The measured signal at each pixel is normalized by the unmodulated optical intensity. The normalized magnitude at pixel (x,y) is

$$I_{\mathrm{IF\_norm}}(x,y,t) = \frac{I_{\mathrm{IF}}(x,y,t)}{I_0(x,y)}, \tag{8}$$

#113871 - $15.00 USD Received 7 Jul 2009; revised 2 Aug 2009; accepted 7 Aug 2009; published 19 Aug 2009

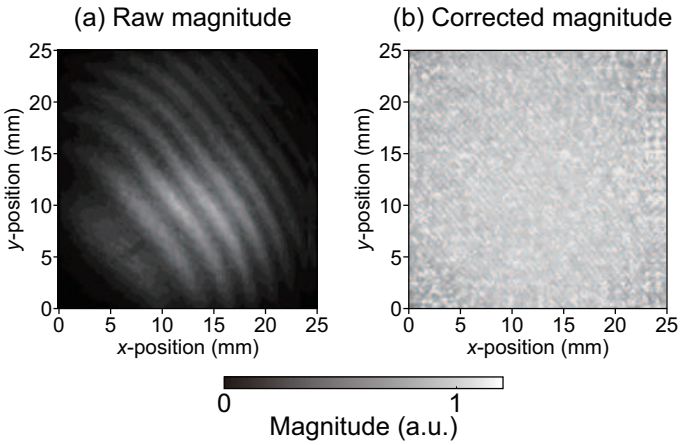

Fig. 4. (a) Raw and (b) corrected magnitude images of modulated light at 5 kHz. The number of accumulated frames was 8192.

where $I_{\mathrm{IF}}(x,y,t)$, $I_{\mathrm{IF\_norm}}(x,y,t)$, and $I_0(x,y)$ are the measured signal magnitude, the normalized signal, and the input light power at pixel (x,y), respectively. As a result, the sensitivity fluctuation of the illuminated beam profile is canceled and the artifact is reduced. Figure 4 shows measured field magnitude images with and without correction. In this measurement, intensity modulated at a frequency of 5 kHz was launched into the LEI optics. An aluminum mirror was used in place of the electro-optic sensor. The modulation amplitude was approximately 0.001, which corresponds to 1 least-significant bit (LSB) of digital output signal from the image sensor. In the raw magnitude image, Fig. 4(a), the signal magnitude at the center is higher than at the periphery because the input beam has a Gaussian profile. Also fringes are observed due to the cavity structure consisting of the sensor and cover glass. When an EO sensor plate is inserted, other fringes appear. Figure 4(b) shows the corrected magnitude image. The input beam profile is obtained without optical modulation. By the magnitude correction, the nonuniformity is reduced.

3.3. Phase correction

The CMOS image sensor uses a rolling shutter. A row in the sensor is scanned sequentially, so that the exposure timing differs from row to row. That results in an artifact in the phase image. Figure 5 shows phase images acquired under the same conditions as in Fig. 4. The row is parallel to the horizontal axis. In Fig. 5(a), without phase correction, a step-like artifact is observed. In the image sensor, four rows are read simultaneously, so that a step appears after every fourth row. Because the difference in exposure timing is determined by the sensor clock, the artifact can be eliminated by image correction. The corrected phase is

$$\phi_{\mathrm{cor}}(x,y) = \phi_{\mathrm{raw}}(x,y) + \Delta\phi \cdot (y \div 4), \tag{9}$$

where $\phi_{\mathrm{raw}}(x,y)$ and $\phi_{\mathrm{cor}}(x,y)$ are the measured and corrected phase signals at pixel (x,y), respectively, and $\Delta\phi$ is the phase difference between each set of four rows. The symbol $\div$ denotes integer division. Figure 5(b) is the corrected image, having a uniform phase distribution. The phase image shows the relative phase distribution in the observed area.

#113871 - $15.00 USD Received 7 Jul 2009; revised 2 Aug 2009; accepted 7 Aug 2009; published 19 Aug 2009

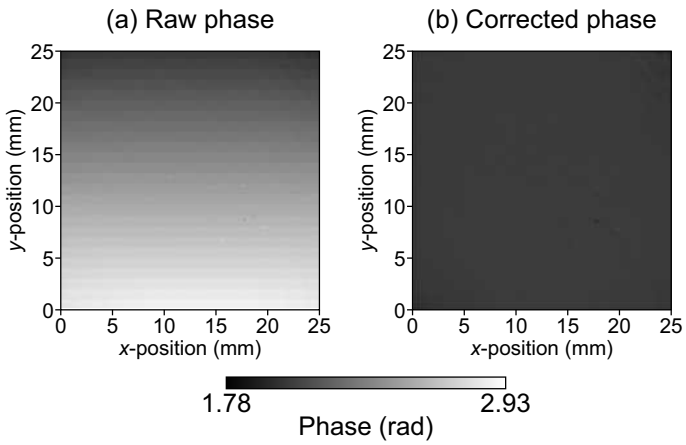

Fig. 5. (a) Raw and (b) corrected phase images of modulated light at 5 kHz. The number of accumulated frames was 8192.

4. Characterization of the modulated signal detection

To evaluate the sensitivity of the signal detection by the high-speed image sensor, the output value after signal processing by the DSP and PC is plotted as a function of modulation amplitude in Fig. 6. The input light is modulated at 5 kHz. The horizontal axis is the modulation amplitude of the A/D converted waveform, calculated from the input modulated light. The vertical axis is the average value of 5×5 pixels around the pixel having the highest received power. The results show that the detected signal magnitude is proportional to the square of the input modulated light. In this case, the minimum detectable signal magnitude is lower than 1 LSB.

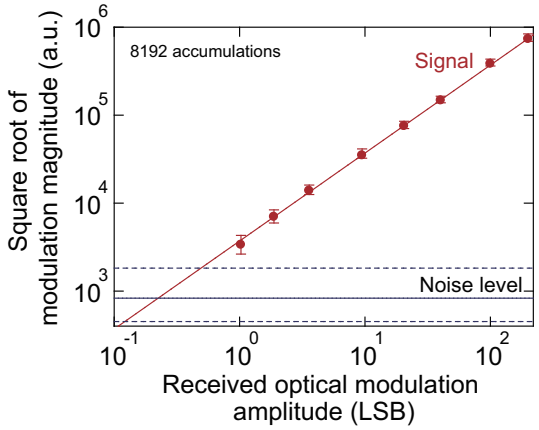

Fig. 6. Square root of the signal magnitude as a function of the optical modulation amplitude at the image sensor. The modulation amplitude is a digital value output from the image sensor. The plotted value is the average of 5×5 pixels.

Figure 7 plots the relation between the output value and the accumulation number. The linearity indicates that the image frames and the reference RF synthesizer are well synchronized, and that the phase shift during the image acquisition, which is 0.4096 s (50 μs $\times$ 8192 frames), is sufficiently low. On the other hand, the average magnitude of the noise is proportional to the

#113871 - $15.00 USD Received 7 Jul 2009; revised 2 Aug 2009; accepted 7 Aug 2009; published 19 Aug 2009

accumulation number N. Therefore, the S/N ratio increases with the accumulation number as long as the accumulation time is shorter than 0.4096 s.

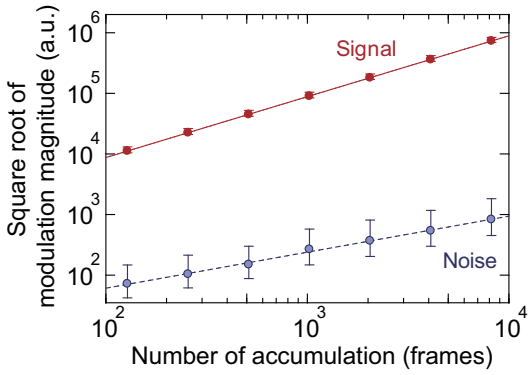

Fig. 7. Square root of the signal magnitude as a function of the number of accumulated frames. The optical modulation amplitude received by the image sensor is approximately 200 LSB. The magnitude value is the average of 5×5 pixels.

5. Demonstration of LEI

By using the LEI system, intensity and phase distribution images of RF electric fields are obtained in real time for an arbitrary measurement frequency. These features enable electric field observations that have not been previously realized. In this section, some example movies are shown.

5.1. Imaging of moving objects

The system enables real-time observations of electric-field variations in the vicinity of a device under test (DUT) in operation. For example, by translating the DUT, points where the electric field is high can be quickly located.

For use as a DUT, we prepared a simple cavity made of a micro-strip line with two gaps as shown in Fig. 8. The measurement frequency was set at 3.7 GHz, which is a resonant frequency of the cavity including the ZnTe plate placed over the DUT The input signal power was 22 dBm. The output end of the DUT was terminated with a 50-Ω terminator. The EO sensor was a (100) ZnTe crystal plate. The spacing between the EO sensor and the DUT was approximately

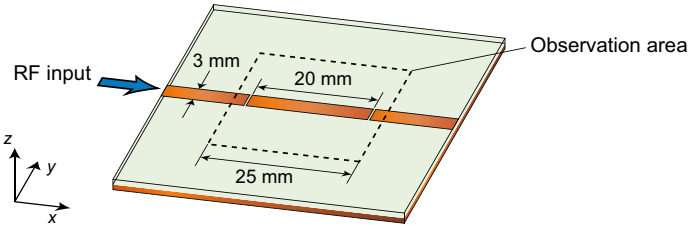

Fig. 8. Schematic of a micro-strip line bandpass filter. The dashed square is the observation area. The substrate is made of FR-4.

#113871 - $15.00 USD Received 7 Jul 2009; revised 2 Aug 2009; accepted 7 Aug 2009; published 19 Aug 2009

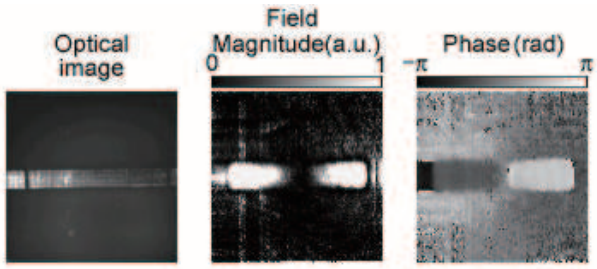

Fig. 9. Movie of the optical image, field magnitude, and phase of the electric field near the MSL bandpass filter (Media 1). The RF frequency and power input into the filter were 3.7 GHz and 22 dBm, respectively. The number of accumulations was 4096 and the frame rate was 5 frames per second.

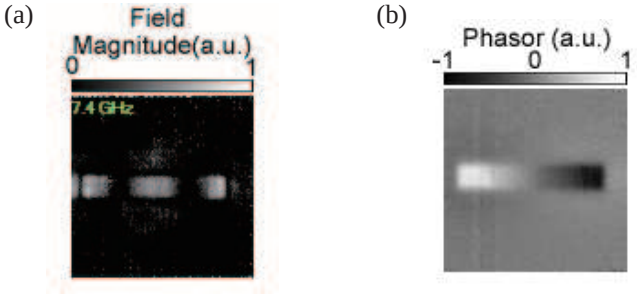

Fig. 10. Movies of the electric field above the MSL resonator. (a) Field magnitude pattern while the RF signal frequency is swept from 1.0 to 10 GHz in (Media 2). (b) Electric field phasor pattern at 3.7 GHz for a phase rotation frequency of 0.2 Hz. The input power into the filter was 22 dBm for (Media 3). The number of accumulations was 4096.

0.3 mm. The detected electric field magnitude and phase images are shown in Fig. 9 (and the accompanying movie). The field magnitude contrast is intentionally increased to observe the electric field around the cavity. As the DUT is translated, the electric field corresponding to the DUT moves. The frame rate of the image sensor was 20 kHz and the number of accumulated frames was 4096. Thus, the electric field magnitude and phase were determined with a frame rate of 2.5 frames / s. These images reveal that the electric field at both ends of the cavity is relatively intense, with opposite phase. In the movie, the phase rotates slightly for 18 s, indicating that more precise phase locking is required for long time observations.

5.2. Frequency and phase sweep

The measurement frequency is determined by the local oscillator frequency f_{LO} and the intermediate frequency f_{IF}. By sweeping f_{LO}, the electric field variation with frequency can be observed as shown in Fig. 10(a). The same DUT was used as in the previous section.

The input power from the signal source at $f_{\mathrm{RF}}(= f_{\mathrm{LO}} + f_{\mathrm{IF}})$ was set to 23 dBm. The frequencies f_{LO} and f_{RF} were swept simultaneously so that thier difference was fixed to 5 kHz, which corresponds to the intermediate frequency f_{RF}. If the frame rate of the image sensor is not synchronized to the intermediate frequency signal, no electric field image is obtained. The movie shows that standing waves are exited in the cavity at the 1st and 2nd resonant frequencies of 3.7 and 7.4 GHz, respectively. As the frequency increases, the sensitivity becomes low because

#113871 - $15.00 USD Received 7 Jul 2009; revised 2 Aug 2009; accepted 7 Aug 2009; published 19 Aug 2009

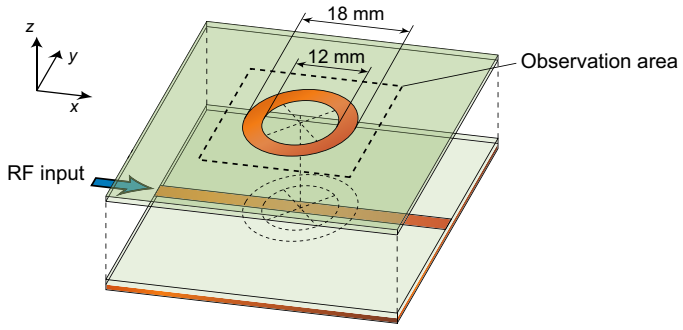

Fig. 11. Schematic of the ring cavity and MSL. In the experiment, there was no gap between the ring and micro-strip line boards.

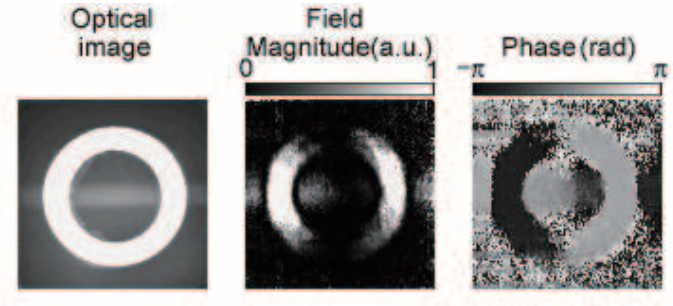

Fig. 12. Movie of the optical, field magnitude, and phase images of the electric field above the MSL bandpass filter. The input power into the filter was 23 dBm for (Media 4). The number of accumulations was 4096 and the frame rate was 5 per second.

the modulation efficiency of the Mach-Zehnder modulator decreases and the loss of the transmission lines increase. In this experiment, the intermediate frequency value is chosen from the maximum frame rate of the image sensor and the intensity noise spectrum of the laser source. At the higher intermediate frequency, the lower laser intensity noise is obtained. However, the signal-to-noise ratio of the image sensor used in this system is significantly lower.

By adjusting the difference between f_{IF} and the reference frequency to a nonzero value lower than the frame rate, the electric field variation with the phase can be measured. Figure 10(b) shows a phasor image during phase rotation. The power and frequency of the RF input signal were 22 dBm and 3.7 GHz, respectively, with a period of phase rotation of 5 s. Signal oscillations at the antinodes at both ends of the cavity are clearly observed.

5.3. Environmental variations

When RF circuits are placed close together, their electric near-fields are coupled. Such an electric field coupling can be observed by the LEI system.

We prepared a two-layer device made of a ring and a micro-strip line as shown in Fig. 11. The substrate of both layers is 1.6-mm-thick FR-4. The width of the ring and micro-strip line is 3 mm, and the diameter of the ring is 18 mm. The spacing between the EO sensor and the DUT was approximately 0.3 mm. The RF power and frequency were 3.0 GHz and 23 dBm. Figure 12 shows the electric fields while the micro-strip line was moved. Because the substrate

#113871 - $15.00 USD Received 7 Jul 2009; revised 2 Aug 2009; accepted 7 Aug 2009; published 19 Aug 2009

is semi-transparent, the position of the micro-strip is observed in the optical images. The results show that the electric field is coupled to the ring when the micro-strip line intersects the axis of the ring. A standing wave with two nodes is observed. This method could be useful to find malfunctions when the environment changes.

6. Conclusion

We developed a 100×100-pixel real-time lock-in detection system based on a high-speed and high-sensitivity CMOS image sensor and a DSP. A sinusoidal optical signal at 5 kHz was successfully detected with the system. The sensitivity to optical modulation amplitudes is approximately 1 LSB at 14-bit resolution, corresponding to a dynamic range of 84 dB, with an accumulation time of 0.4096 s when averaging over 5×5 pixels. By using this system, we also demonstrated real-time microwave electric field imaging based on parallel photonic heterodyning. Pairs of electric field magnitude and phase images can be detected in real-time . These features should be applicable to the diagnosis of microwave circuits/devices. The LEI system demonstrates the potential of the image sensor and the DSP. Further improvement of the frame rate and dynamic range of image sensor would make the LEI system more practical. It is expected that the lock-in imaging system can be used for not only the LEI system but other parallel optical measurement systems.

Acknowledgements

The authors thank Mr. Ryohei Ikeno of Stanley Electric Company and Ms. Kiyo Murano of Brainvision for their technical support. The authors also thank Mr. Shinichi Shirasu and Dr. Yuichi Matsushima of the National Institute of Information and Communication Technology (NICT), and Prof. Jun Ohta of the Nara Institute of Science and Technology (NAIST) for their assistance. This work was supported by the Strategic Information and Communications R&D Promotion Programme (SCOPE) from the Ministry of Internal Affairs and Communications.

#113871 - $15.00 USD Received 7 Jul 2009; revised 2 Aug 2009; accepted 7 Aug 2009; published 19 Aug 2009